applied sciences

MDPI

Article

Comparative Analysis of Cooling Methods for Dynamic Infrared Thermography (DIRT)-Based Skin Cancer Diagnosis

Jan Verstockt [1,*], Filip E. F. Thiessen [2,3], Isabelle Hoorens [4], Lieve Brochez [4] and Gunther Steenackers [1]

[1] InViLab Research Group, Department of Electromechanics, Faculty of Applied Engineering, University of Antwerp, Groenenborgerlaan 171, B-2020 Antwerpen, Belgium
[2] Department of Plastic, Reconstructive and Aesthetic Surgery, Multidisciplinary Breast Clinic, Antwerp University Hospital, University of Antwerp, Wilrijkstraat 10, B-2650 Antwerp, Belgium
[3] Department of Plastic, Reconstructive and Aesthetic Surgery, Ziekenhuis Netwerk Antwerpen, Lindendreef 1, B-2020 Antwerp, Belgium
[4] Department of Dermatology, Ghent University Hospital, C. Heymanslaan 10, B-9000 Ghent, Belgium
* Correspondence: jan.verstockt@uantwerpen.be

Abstract: Skin cancer is a significant global health issue, placing a growing burden on individuals and society. Conventional diagnostic methods like visual examination and biopsy have limitations in invasiveness and accuracy. As a result, alternative tools such as infrared thermography have gained attention in skin cancer diagnosis. Tissue-mimicking phantoms have been instrumental in facilitating research in this field, offering controlled environments. While they do not fully replicate human skin complexity, physical skin models provide stability, ease of fabrication, and control over properties. Agarose phantoms are employed in this study. This research focused on testing and comparing cooling techniques for human skin in the context of skin cancer diagnosis using dynamic infrared thermography. Six cooling methods were investigated: a cool pack, an aluminum medal, ice, alcohol, a vortex cooler and a Zimmer Cryo 6 cooler. The experimental setup involved an infrared camera (Optris Xi400) with microscope optics positioned above an agar phantom mimicking flat skin and an ulcerating skin lesion. Based on experiments conducted on the skin phantom, it was observed that convective cooling methods offered more consistent and uniform cooling. Conversely, conductive methods proved effective for flat objects but posed challenges in achieving uniform cooling for bulging skin or ulcerated lesions. Ice or alcohol were deemed unsuitable due to artifacts influencing the infrared radiation and thermal camera view. A decision matrix assessed cooling techniques based on criteria such as uniformity, repeatability, view obstruction, efficiency, workload, patient comfort, clinical suitability, noise exposure, consumables, additional equipment, and price. The Zimmer Cryo 6 cooler emerged as the most suitable cooling method after evaluating various factors.

Keywords: infrared thermography; skin cancer; cooling; skin-mimicking phantom; agarose gel; finite element model

Citation: Verstockt, J.; Thiessen, F.E.F.; Hoorens, I.; Brochez, L.; Steenackers, G. Comparative Analysis of Cooling Methods for Dynamic Infrared Thermography (DIRT)-Based Skin Cancer Diagnosis. *Appl. Sci.* **2023**, *13*, 10105. https://doi.org/10.3390/app131810105

Academic Editor: Igor Pušnik

Received: 11 July 2023
Revised: 4 September 2023
Accepted: 7 September 2023
Published: 7 September 2023

1. Introduction

1.1. Skin Cancer

Cancer is the first or second leading cause of premature death in 134 of 183 countries (i.e., ages 30–69) [1]. In 2020, more than 19 million new cases of cancer were diagnosed, and approximately 10 million deaths are expected [2]. According to the World Health Organization, the total annual economic cost of cancer is estimated to exceed 1 trillion euros [2]. These figures are expected to continue to rise due to increasing population and life expectancy. Cancers of the skin are the most common cancer type in humans. The incidence of specifically both melanoma and non-melanoma skin cancers is increasing worldwide, especially in the older White and Asian populations due to the exposure to ultraviolet light (sun exposure) [3]. Melanoma incidence rates have tripled in Europe over the past four decades, similar to the United States. Early detection and treatment of skin cancer

can improve outcomes while having less impact on the quality of life of the patient while the mortality rate is decreased. However, traditional methods of skin cancer diagnosis, such as visual examination and biopsy, can be invasive and may not detect all cases of skin cancer [4].

Skin cancer screening now commonly includes a total body skin examination (TBSE) in which dermatologists use non-invasive methods like dermoscopy to differentiate between malignant and benign skin lesions [5]. The diagnosis of melanoma is typically made through the use of the ABCDE classification, which stands for Asymmetry, Border irregularities, Color differences, large Diameter, and Evolution over time [6]. However, even when performed by skilled dermatologists, this method has a relatively low specificity and moderate sensitivity [7]. Dermoscopy with polarized light can improve sensitivity and specificity, but invasive excisions are still often necessary to exclude false-negative findings [8]. Other non-invasive approaches for cancer diagnosis include for example confocal microscopy, multispectral imaging, and photoacoustic imaging… [9]. CT/PET are invasive approaches as they make use of X-rays and/or contrasting or radioactive liquid.

The purpose of this article is to give an overview of the different skin-cooling techniques for dynamic infrared thermography skin cancer diagnosis that are used in the literature. Over time, researchers used a diversity of skin cooling techniques in their research to diagnose skin cancer with infrared thermography. The different cooling techniques are tested on a human skin–tissue-mimicking phantom to be able to compare them accurately. The cooling effect of the different techniques is visualized and monitored with an infrared camera and thermistors to find the optimal cooling technique.

1.2. Skin Cancer and Infrared Thermography

Active infrared thermography (IRT) is a non-invasive diagnostic tool that uses infrared radiation to measure the temperature of the skin. Thermography can detect temperature changes and distribution on the surface of the human body [10]. Infrared emissions from human skin at 27 °C are in the wavelength range of 2–20 µm and peak at 10 µm. Body infrared rays, a narrow wavelength range of 8–12 µm, is used for medical applications [11]. Infrared thermography can be categorized into two distinct subtypes: passive thermography and active thermography. Passive thermography involves the examination of the subject in its natural thermal equilibrium without the imposition of external thermal stress. In contrast, active thermography employs a deliberate thermal excitation to enhance thermal contrast. Specifically, in the context of skin cancer detection, active thermography involves cooling the skin cancer lesion to capture its subsequent reheating pattern and rate. More background can be found in previous research [4]. It has been used in medical applications for decades, and it is particularly useful for identifying skin cancer due to the increased metabolic activity and angiogenesis present in malignant cells [12]. Melanoma, specifically, is thought to have a higher temperature than surrounding healthy skin, making it a prime target for infrared imaging [4]. Other skin tumor types, such as basal cell carcinoma, may have a different thermal signature, indicating that thermography can be used to differentiate between various types of skin cancer [13]. Studies have shown that thermal infrared imaging can detect new blood vessels and chemical changes associated with tumor development and growth [14,15]. Infrared thermography boasts a distinct advantage over alternative imaging methods: its ability to discern the rate of skin rewarming, facilitating precise assessment of both the boundaries and depth of a skin lesion as outlined in [16]. Additionally, this technique eschews the use of ionizing or detrimental radiation, relying solely on the body's intrinsic heat for imaging purposes.

1.3. Skin-Mimicking Phantoms

To overcome the difficulties and ethical problems of conducting studies on living organisms, tissue-like phantoms are used. Traditionally, experiments are conducted on animals, humans, cadavers, and ex-plants to study tissue interactions [17]. Experiments on human and animal skin are difficult to perform because of the wide variability in skin

composition. Because of the ethical problems and variability in composition, research on tissue-like phantoms is increasing. One of the main advantages of using skin tissue phantoms is that they provide a controlled and reproducible environment for experimentation, which is difficult to achieve with human subjects. Over the years, an extensive amount of literature has been published on tissue phantoms for various applications [18–23].

Commercially available cultured in vitro skin tissue cells are a possibility for use in research or for clinical purposes. However, there are significant difficulties in preparation, handling, storage, and standardization [19]. The use of in vitro tissue models for thermographic studies under realistic physical conditions is very difficult. The physical properties of such in vitro models are too different from those of real skin and are characterized by large variations [17].

Physical skin models are stable over the long term, are easy to fabricate, store and manipulate, and also have better control over their physical properties. The high repeatability and reliability of physical model parameters can be achieved without having to worry about ethical issues [17]. However, skin tissue phantoms have some limitations like the lack of blood flow and cellular response and the difficulty in mimicking the complex structure and composition of human skin. Additionally, skin tissue phantoms are typically much simpler than actual human skin: they are customized to mimic specific skin conditions, which can limit their ability to accurately replicate the behavior of human skin.

The structure of human skin is divided into three layers: the epidermis, dermis (papillary and reticular), and hypodermis [24]. The epidermis is the thin uppermost layer mainly composed of migrating keratinocytes that eventually form the outermost layer, which is known as the stratum corneum [25]. The dermis, which is divided into the papillary dermis and the reticular dermis, provides structural strength to the skin. The hypodermis, located beneath the dermis, acts as a fatty layer that protects the body from mechanical impact, heat, and cold [26].

When constructing a tissue-mimicking phantom for thermal analysis, two crucial parameters to consider are the specific heat capacity c in $(\mathrm{J} \cdot \mathrm{kg}^{-1} \cdot \mathrm{K}^{-1})$ and the thermal conductivity k in $(\mathrm{W} \cdot \mathrm{m}^{-1} \cdot \mathrm{K}^{-1})$. The properties of human skin tissue vary depending on the individual and the location of the body. For instance, the thickness of the epidermis (uppermost layer) can range from 0.45 to 2 mm [27].

Cetingül and Herman [24] reported ranges of thermophysical properties used in their research on a tissue-simulating phantom and a finite element heat transfer model of the skin. In addition to specific heat capacity c and thermal conductivity k, other parameters like the blood perfusion rate ω_b in the skin layers, metabolic heat generation (Q) of different skin layers, and layer thickness h also influence the surface temperature response [24].

Human skin consists of several highly inhomogeneous and anisotropic materials. The skin is one of the largest organs of the human body and actively exchanges mass and heat with the human body and environment, which makes this a very big and complex active open system [17,28,29]. Physical skin models are strong simplifications which try to imitate certain parameters or a combination of parameters of the skin. Depending on the area of research, a physical skin model can consist of different combinations of materials, structures and morphologies. The most common types of physical skin models are based on liquid suspensions, gelatinous substances, elastomers, resins, metals, and textiles with nano-fillers and micro-fillers [17,19]. According to the literature written by Dabrowska et al. [17], the following materials can be used to mimick skin thermal properties: hydrogels, elastomers, metals and textiles. Metal-based skin models are most used to probe the thermal properties of clothing [30]. Textile-based skin models are used to mimick the sweating and mechanical and frictional behavior of the human skin [31,32]. Elastomer tissue-mimicking phantoms are based on the use of silicones or polyurethanes combined with additives like carbon black or titanium dioxide to tune the properties of the elastomers. Silicones and polyurethanes have a long stability and can be tuned very specifically to obtain certain parameters needed for that application. The elastomer models can be molded into different anatomical shapes. Hydrogel-based skin phantoms consists mostly of gelatin,

agarose models and polyvinyl alcohol gels [18]. A hydrogel-based phantom encapsulates water as a main component and forms a stiff matrix that limits water mobility. The human skin tissue-mimicking phantom used for our experiments is based on a hydrogel phantom, more specifically an agarose-based skin phantom. Agar is a gelatin-like substance made from seaweed polysaccarides [17]. Agarose skin models are not very stable in the long term and have limited shelf life, but they are versatile as well as easy to use and produce. The acoustic, thermal and physical properties are similar to those of human skin and thus widely used for the fabrication of thermal phantoms [19]. The thermal characteristics of the model can be altered by changing the composition of the mixture. Agarose skin phantoms are easily fabricated by heating a mixture of agarose powder and deionized water above 85 °C, mixing thoroughly and pouring the mixture into a mold. At room temperature, the model resembles a lightly opaque gelatinous substance [33]. In the literature, a range of different compositions of the agar phantoms are used. Ambastha et al. used a 1% research grade agar and distilled water solution to simulate human brain soft tissue [34]. A human skin tissue phantom used by Cetingül and Herman is based on a composition of 4% solution of agar and distilled water to match the thermal properties of human skin [35]. Kumari et al. developed a gel phantom with a 0.6% agar solution dissolved in distilled water to quantify skin necrosis during cryotherapy [36]. The thermal conductivity of their 0.6% gel phantom is 0.58 (W/m · K) (error = 0.0037). Cho et al. conducted an experiment where the thermal conductivity and specific heat are varying depending on the agar–gel concentration [37]. The composition of the agar–gel was 0.5%, 1.5%, 2.5%, 3.5% and 5% with, respectively, a thermal conductivity in (W/m · K) of 0.7749 ± 0.124, 0.667 ± 0.116, 0.591 ± 0.145, 0.404 ± 0.171 and 0.379 ± 0.113. The specific heat c in J/kg · K for the 1.5%, 2.5%, 3.5% and 5% agar mixtures is, respectively, 6465 ± 452, 5827 ± 218, 4887 ± 477 and 4011 ± 386. The thermal conductivity of agarose hydrogel resembles, according to Hou [38], 0.65 (W/m · K) and decreases slightly to 0.51 (W/m · K) with the concentration increase from 0.5 wt% to 2 wt% of concentration.

1.4. Previous Research on Skin-Cooling Techniques for Dynamic Infrared Thermography

In laser dermatology, to protect the epidermis in laser dermatology applications, the two most popular methods for skin cooling are spray cooling with tetrafluoroethane (boiling point −26 °C) and contact cooling (−27 °C sapphire plate). With the spray and contact cooling, the basal skin layer is cooled down to be between −5 and 5 °C. These cooling methods must be carefully controlled to prevent irreversible skin damage caused by local skin freezing [39]. Spray and contact cooling provide efficient skin cooling for laser dermatology applications, but due to the possible serious skin damage, especially on critical skin lesions, it is not suited for dynamic infrared thermography on skin cancer lesions. Cheng and Herman [40] performed a computational analysis of different skin-cooling techniques on a human skin model based on the Pennes bioheat equation. The skin lesions in this study are defined by an invasion depth of less than 4 mm. The cooling methods they considered are constant temperature cooling, water-soaked cotton and convective cooling. The constant temperature cooling method is an idealized case of conduction cooling: the temperature of the coolant remains constant during cooling, which is difficult to achieve in practice. The second cooling method studied in their work is cooling with a cotton patch soaked in water. Cheng modeled the water-soaked cotton patch as a 2 mm-thick layer of water in direct and ideal contact with the skin. Their third cooling case is based on convective cooling by air, varying the convective heat transfer coefficient and the temperature of the air. The thermal penetration depth of the three cooling cases are compared for a cooling temperature of 4 °C, 12 °C and 20 °C. Cheng and Herman concluded that cooling at 20 °C is a suitable cooling temperature that allows the cooling effect to reach a lesion depth of 4 mm within 2 min.

Strakowksa et al. [41] also experimented with different cooling methods to find the most convenient cooling method for infrared thermography on skin diseases. In their experiments, they tested different methods: cooling by gel, metal medal with 6 s of skin

contact or compressed air. The application of compressed air showed that the temperature is not controllable because the compressed air is not conditioned properly. Cooling by gel is possible if the disease covers a small area. The application of the cooling gel will interfere with the accuracy of the thermographic readings due to the change in emissivity. The use of the metal block is most suitable for their experiments, but the field of view during cooling is obstructed.

Buzug et al. [42] used a conductive cooling method with cooled gel packs. An area of 10 cm by 10 cm is cooled to 20 °C. They mentioned that the recording protocol needs improved standardization due to the patient-individual variation of the acquisition conditions. Santa Cruz et al. [43] use immersion in water at 15 °C for 2 min. When immersion in water was not possible, forced evaporation with an alcohol spray and fan currents was used. They concluded that a non-contact system using cold air currents was necessary to collect qualitative data without damaging the skin or causing changes in skin permeability. Cetingül et al. [44] introduced cooling with a stream of cold air from a vortex tube for a period of one minute. Compressed air (from an air tank or air compressor supply lines) must be present for the vortex tube to operate. An area with a diameter of 5 cm is cooled by the outlet of the vortex tube, but the cooling temperature is not mentioned in their work. Controlling the outlet temperature of a Ranque–Hilsch vortex tube is difficult to achieve; the outlet temperature is pressure, flow and ambient temperature dependent. The outlet temperature of the vortex tube is not yet constant in the initial seconds of cooling initialization. The produced acoustic level of the vortex tube, which can range between 80 and 130 dB, is another crucial factor to consider [45]. Godoy et al. [46,47] proposed a standardized analysis protocol for active thermography that compensates for deficiencies in the cooling process. They continued to work on the research of Cetingül et al. and used a Ranque–Hilsch vortex tube as the initial cooling unit. They later replaced the cooling unit with a commercial air-conditioner because it is portable and provides a constant flow of conditioned air. In their work, no cooling temperature is specified for the conditioned air flow. Magalhaes et al. [48] used an aluminum medallion with a diameter and height of 50 mm and 20 mm, respectively, for thermal provocation of 1 min; the temperature of the cold provocation is not mentioned. Gomboc et al. [49] modeled and designed a constant temperature cooling device for melanoma screening. The device is based on an active cooling device that uses a Peltier module and a metal disk to achieve a constant cooling temperature by conduction and to induce deep cooling. Bonmarin et al. [50] presented a lock-in thermal imaging setup for a proof-of-concept study on benign lesions. The temperature-modulated airflow was achieved by using a cryogenic cold air device (Cryo 6, Zimmer Medizin Systeme, Ulm, Germany). The Cryo 6 cooling system cools the skin in a non-contact, rapid and reproducible manner without affecting the infrared camera's field of view or interfering with it. Bonmarin et al. [51] suggest that convective heat transfer is likely the best thermal excitation method for dermatological applications. This method allows for the regulation of airflow temperature and the application of relatively large temperature gradients. Moreover, the skin surface temperature can be easily monitored with an IR camera without any obstructions thanks to convective heat transfer. This non-contact thermal excitation method is hygienic and optimal for clinical devices.

2. Materials and Methods

The aim of this work is to test different cooling techniques which can be applied to human skin. A comparison between the different cooling methods is made, and in the end, the best suitable cooling method for skin cancer diagnosis based on dynamic infrared thermography is selected. The experimental measurement setup, skin-mimicking phantom, measurement protocol and comparing methods are described in the following section.

2.1. Skin-Cooling Techniques

Six different cooling techniques are tested and compared in this study and are divided into three categories based on the heat transfer method: convection cooling, conduction

cooling and evaporative cooling. Thermal radiation is not taken into account, since no cooling method based on this principle is used. Conduction cooling and evaporative cooling are direct contact cooling methods; contact with the skin is necessary to apply the thermal provocation. Convection cooling, as is the case in cooling with air, is a contactless method of thermal provocation. Submersion in water is another convective heat transfer technique used by Santa Cruz [43], but the agar skin phantom is not able to withstand immersion in water as it will swell, considerably absorbing water and causing a change in the composition and thermal properties. Thus, water cooling is also excluded from this research.

2.1.1. Evaporative Cooling

The evaporative cooling technique used in this comparison is introduced by Santa Cruz et al. [43]. Rubbing alcohol is sprayed on the skin followed by fan currents that induce cooling by forced evaporation.

2.1.2. Conductive Cooling

The first cooling method based on conductive heat transfer is an aluminum medal for thermal provocation based on the research of Magalhaes [48]. The aluminum medal is a square bar with a length and width of 50 mm and height of 20 mm at a temperature of 15 °C. The second conductive cooling method uses a cooled gel pack as used by Buzug et al. and Burkes et al. [13,42,52]. The temperature of the cold pack is 15 °C. The third cooling method is cooling with ice.

2.1.3. Convection Cooling

The first convective cooling method, as implemented by Godoy and Cetingul and Herman, uses a Ranque–Hilsch vortex tube to provide the cold air flow [46,47]. It is important to mention that a steady and controlled temperature output of the vortex tube is rather difficult to obtain due variations in the pressured air supply, temperature of the pressured air and the time to obtain a steady-state flow and temperature. The second convective cooling device is a cryo cooler Cryo 6 by Zimmer (Zimmer Medizin Systeme, Ulm, Germany). The airflow generated by the Cryo 6 device has a temperature of −30 °C and can be regulated in 9 airflow levels up to 1000 L/min. The airflow is filtered, moisture-free, oil-free and quiet [53]. Airflow levels 1, 3 and 5 are used in this research to measure the influence and cooling penetration.

2.2. Experimental Setup

2.2.1. Infrared Camera

The used thermal camera is an Optris Xi400 with microscope optics (Optris GmbH, Berlin, Germany) long-wave infrared camera (8–14 µm). The type of detector is an uncooled microbolometer with a pixel pitch of 17 µm and a thermal sensitivity (NETD) of <80 mK. The thermal camera is equipped with manual motor focus and microscope optics (18° × 14°) with a minimal focus distance of 90 mm and maximum focus distance of 110 mm. The setup is shown in Figure 1. The thermal camera is used to capture 16-bit RAW thermal image sequences in 382 × 288 resolution at a frame rate of 27 Hz. Microscope optics specifically allows focusing extremely close on a subject such that tiny details from the skin lesion become prominent features with high resolution. A one-point non-uniformity correction (NUC) is applied on the raw images at a reference temperature of 15 °C using a blackbody. The infrared camera was positioned at 100 mm above the tissue-mimicking phantom. The field of view at the object surface is 34.2 mm × 25.7 mm with a pixel size of 90 µm and a 3 × 3 pixel size of 0.27 mm.

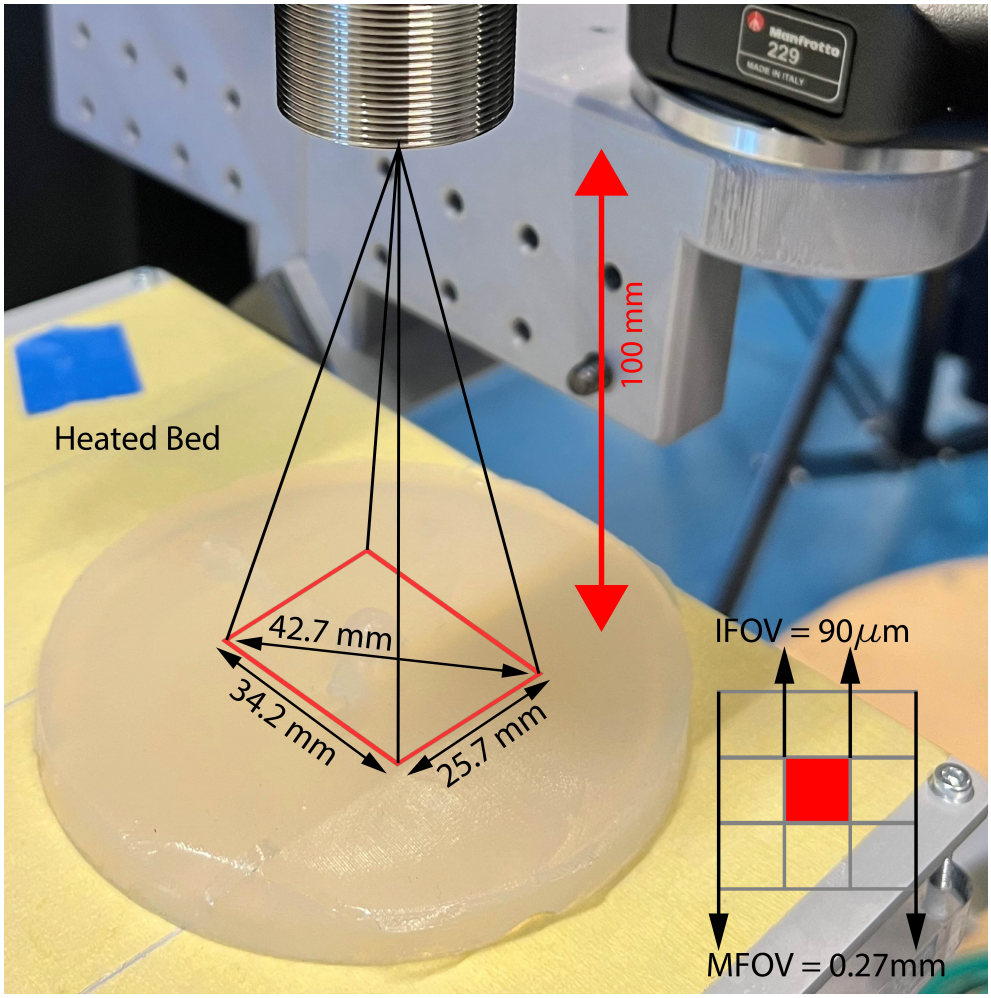

Figure 1. Camera setup with an Optris Xi400 microscope optics thermal camera placed at 100 mm above the skin phantom surface. The field of view at the object surface is 34.2 mm × 25.7 mm with a pixel size or Instantaneous Field of View (IFOV) of 90 µm and a Measurement Field of View (MFOV) of 3 × 3 pixels or 0.27 mm.

2.2.2. Skin Phantom

The agar skin phantom for this study is based on the tissue-mimicking phantom used in the research of Cetingul and Herman, as this composition is accurate for thermal modeling [35]. A solution of 4% of lab-grade agar powder (Himedia labs, Einhousen, Germany) and distilled water is used to match the thermal properties of human skin. To create the skin phantom, the process involves dissolving agar powder gradually in distilled water to create a solution with a concentration of 4.0%. This solution, comprising water and agar, is then heated until it reaches the melting temperature of agar, which is 85 to 95 °C [54]. Once melted, the agar solution is carefully poured into molds and left to cool for several hours until it solidifies and takes on a gelatinous texture. The 3D-printed moulds used for this experiment create an agar–agar specimen of cylindrical shape with a diameter of 100 mm and a thickness of 10 mm. Three different molds are used, as shown in Figure 2: a flat mold which resembles flat skin and a second mold which imitates an ulcerating skin lesion. The ulceration has a diameter of 5 mm and a height of 3 mm. The thickness of the ulceration is determined based on the classification by Hout et al. They categorized ulcerated melanoma into two groups: excessive ulcerations (>5 mm or >70%) and minimal/moderate ulcerations (<5 mm or <70%) [55]. The diameter of the ulcerating melanoma, specifically the 5 mm diameter, is determined according to the study conducted by Grande Sarpa et al. [56]. In their research, they classified the data into three categories:

no ulceration, ulceration width ranging from 1 to 6 mm, and ulceration width greater than 6 mm. The skin phantom is placed on an aluminum heated bed and covered with paper tape to decrease the high reflectivity of the aluminum in the infrared spectrum. The temperature of the heated bed is set to 37 °C, which resembles the core body temperature of 37° [42]. To monitor the depth of cooling penetration in the skin phantom for various cooling methods, Platinum Resistance Pt100 Thin Film Detectors (RS Pro) are utilized. These detectors are inserted into the agar substrate. The Pt100 Resistance Temperature Detector (RTD) used in this case has a probe diameter of 1.2 mm and a probe length of 1.6 mm. It has a rapid response time of 0.1 s and is capable of sensing temperatures within the range of −50 to 500 °C. The RTD is connected to a MAX31865 RTD-to-digital converter manufactured by Maxim Integrated. This converter is then connected to an Arduino microcontroller, which utilizes software capable of reading the RTD and temperature values at a frequency of once per second. In this setup, one RTD is inserted into the substrate at a depth of 5 mm, precisely at the center of the lesion. The second RTD is placed at the bottom of the skin phantom, reaching a depth of 9 mm. These detectors provide valuable temperature measurements to track the cooling process and assess the depth of penetration in the skin phantom.

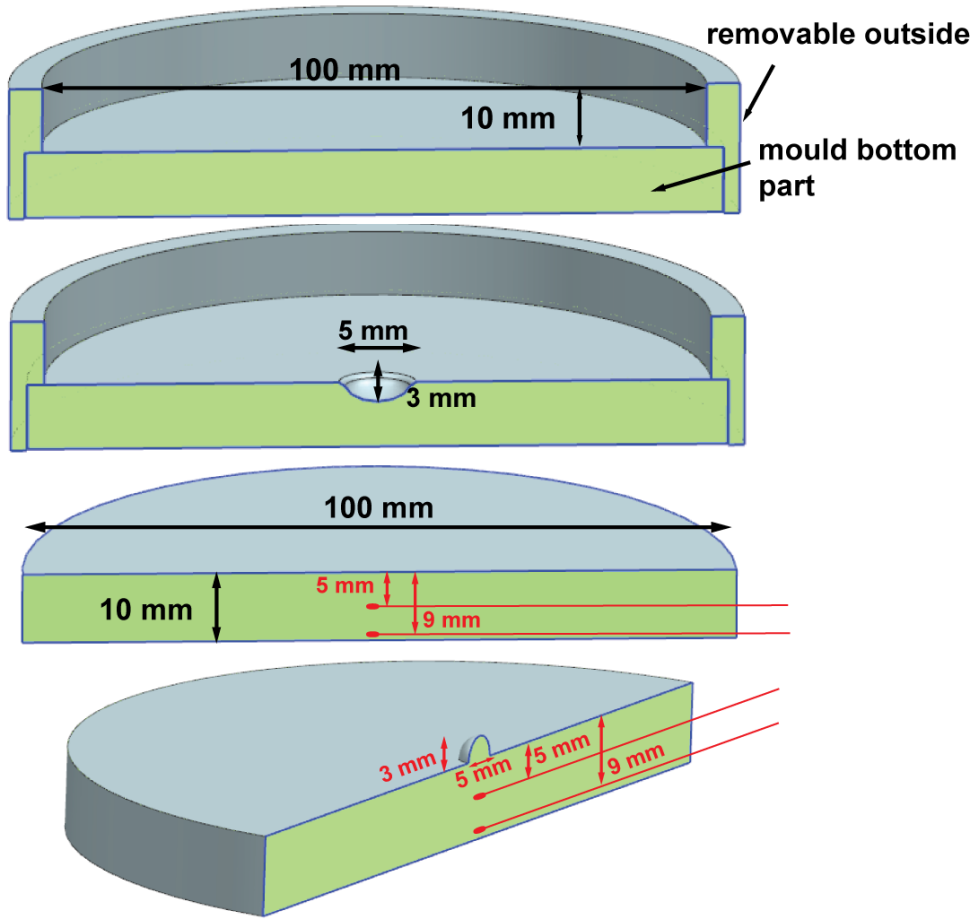

Figure 2. Two molds used to create the agar skin phantoms with dimensions. The mold has the possibility of being taken apart so that the agar gel can be easily removed. The agar phantoms with dimensions and the placement of the two RTDs inside the substrate.

2.3. Measurement Protocol

The thermal camera was prepared to capture the reheating process by positioning it at the center of the skin phantom: precisely at a height of 100 mm. The focus of the camera was adjusted accordingly. The framerate of the camera was set to 27 Hz.

To initiate the experiment, the skin phantom was placed onto a heated bed with a pre-set temperature of 37 °C. Sufficient time was allowed for the skin phantom to reach a steady state and stabilize the thermal conditions at this temperature.

After achieving a steady state, the cooling process was initiated by applying the desired cooling method to the skin phantom. The cooling was maintained for exactly 60 s. If the cooling method did not obstruct the view, such as with the cryo cooler, the thermal camera also captured the cooling process.

Immediately following the cooling period, the reheating process of the skin phantom was captured by the thermal camera. The recording continued for a total duration of at least 240 s.

Once the reheating sequence was completed, the skin phantom was allowed to reach the steady state again. This ensured consistent conditions before repeating the measurement protocol for each cooling method under investigation. All procedures and recording parameters were maintained consistently throughout the experiment. The cooling methods used in this research work are listed below in Table 1.

Table 1. Cooling methods used in this research. The temperature of the evaporative cooling is not determined. The temperature of the Ranque–Hilsch vortex tube depends on the pressure of the compressed air and flow settings of the vortex cooler. The settings were held constant.

Heat Transfer Type	Cooling Method	Temperature
Conductive cooling		
	aluminum medal (50 × 20 mm)	15 °C
	cooled gel pack	15 °C
Evaporative cooling		
	alcohol spray	/
Convective cooling		
	Ranque–Hilsch vortex tube	5 °C
	Zimmer Cryo 6 cooler	−30 °C

2.4. Image Sequence

For each tested cooling method, a thermal sequence is obtained, capturing the cooling load and reheating process. The captured sequences undergo preprocessing, which involves applying a one-point non-uniformity correction (NUC) to the raw images using a blackbody as a reference at a temperature of 15 °C. The preprocessed images are then segmented to identify the region of interest (ROI) within the skin phantom. This step is essential for isolating specific areas for further analysis.

Next, the image sequences are divided into the cooling sequence and reheating sequence. From the reheating sequence, a thermal image taken 5 s (frame 135) into the rewarming phase is selected for further analysis. To effectively demonstrate the non-uniform cooling and cooling artifacts resulting from different cooling techniques, the thermograms are processed using a Python algorithm developed by the author.

The data minima are normalized to a consistent temperature of 10 °C, allowing the images to be shifted to the same temperature while preserving the temperature differences. This approach enables visualization of the images using a consistent color scale. Additionally, a histogram is generated for each cooling method to analyze the distribution of the data. A wide range in the histogram indicates non-uniform cooling, while a narrow spike shape suggests a high concentration of pixels at the same temperature, indicating uniform cooling of the phantom. By conducting a qualitative analysis of the thermograms, it becomes possible to visually observe and distinguish the variations in the applied cooling load.

2.5. Decision Matrix

A decision matrix is a valuable tool for evaluating and comparing different cooling techniques in a systematic and objective manner. By considering multiple criteria and

assigning weights to each criterion based on their relative importance, a decision matrix allows for a comprehensive assessment of the cooling methods under investigation. The matrix typically includes columns representing the various cooling techniques being compared and rows representing the evaluation criteria [57]. These criteria include, in order of importance, uniform cooling, repeatability, obstructing the view, cooling efficiency, workload per patient, patient comfort, use in a clinical setting, noise exposure, consumables and additional equipment and price. The decision matrix and its weights can be seen in Table 2. Each criterion is assigned a score or rating based on its performance for each cooling technique. The rating scale is a scale from 1 to 3. Depending on the type of criteria, 1 means high (or low), 2 means moderate and 3 means low (or high). The scores are then multiplied by the corresponding weight assigned to the criterion to calculate a weighted score for each technique. The weights are assigned from ten (or equal to the number of criteria) to one, and each weight can only be used once. The technique with the highest weighted score indicates the most favorable choice based on the given criteria and their assigned weights. The decision matrix provides a transparent and structured approach to inform decision making, facilitating the identification of the most suitable cooling technique for a specific application. When using a decision matrix, assigning weights to the evaluation criteria is an important step that reflects the relative importance of each criterion in the overall decision-making process. The weights are determined through the stakeholder input method. The weights assigned to the criteria reflect the decision-makers' priorities and preferences. It is also important to acknowledge that the weights can be subjective and may vary depending on the specific context or application [58].

Table 2. Decision matrix.

			Conductive Cooling		Evaporative Cooling		Convective Cooling	
Criteria	**Rating Scale**	**Coefficient**	**Aluminum Medal**	**Gel Pack**	**Ice**	**Alcohol Spray**	**Vortex Tube**	**Zimmer Cryo 6**
Obstructing view of camera during/after cooling	1 = high 2 = moderate 3 = low	**8**	2	2	1	1	3	3
Noise exposure	1 = high 2 = moderate 3 = low	**3**	3	3	3	3	1	2
consumables/additional equipment (e.g., pressured air (air compressor), ice (ice cube maker), alcohol, fridge)	1 = high 2 = moderate 3 = low	**2**	1	1	1	1	1	3
Use in clinical/hospital setting (e.g., sterilizable/disinfectable)	1 = low 2 = moderate 3 = high	**4**	2	2	1	1	3	3
Repeatability (e.g., constant temperature, pressure, flow...)	1 = low 2 = moderate 3 = high	**9**	2	2	2	1	2	3
Price	1 = high 2 = moderate 3 = low	**1**	3	3	3	3	2	1
Workload per patient (e.g., disinfecting, number of actions, application difficulty, measurement time...)	1 = high 2 = moderate 3 = low	**6**	1	1	1	1	2	3
Patient comfort (e.g., applicable on whole body, discomfort, duration...)	1 = low 2 = moderate 3 = high	**5**	2	2	2	1	3	3
Uniform cooling	1 = low 2 = moderate 3 = high	**10**	2	1	1	1	3	3
Cooling efficiency	1 = low 2 = moderate 3 = high	**7**	2	2	3	1	2	3
Total:			20	19	18	14	22	27
Total weighted:			106	96	91	63	132	160

The criterion of utmost importance, assigned a coefficient of 10, is uniform cooling, which is aimed at minimizing cooling artifacts that may result in incorrect diagnostics.

Following closely is the criterion of cooling repeatability, ensuring consistent cooling throughout the entire measurement process and across different measurements. The third significant criterion is the obstruction of the field of view, where some obstruction is permissible during the cooling phase, but a clear, unobstructed view is required during the reheating sequence.

The criteria of price, consumables/additional equipment, and noise exposure were assigned the lowest coefficients in the decision matrix. The price factor considers the cost of the devices, with the Zimmer Cryo 6 being relatively expensive compared to other cooling methods but relatively low compared to other medical devices. Although the cost may be higher, it remains within an acceptable range for medical equipment. The criterion of consumables/additional equipment assesses the impact on feasibility, particularly in settings without adequate facilities. However, since the device is intended for use in a clinical setting, the incorporation of necessary consumables or additional equipment becomes more feasible. Therefore, the negative impact of consumables/additional equipment on feasibility can be managed effectively. Noise exposure, the third criterion, can potentially affect the well-being of patients. However, specific measures can be implemented to mitigate noise levels and minimize any adverse effects. By implementing appropriate noise reduction techniques, the potential negative impact on patients' well-being can be mitigated effectively. It is worth noting that despite their lower coefficients, these criteria should not be disregarded entirely. Table 2 presents the remaining criteria for evaluation.

3. Results

The initial section presents the results obtained from the flat agar skin phantom, offering a comprehensive overview of various cooling methods and their associated challenges. Subsequently, the findings from measurements conducted on the ulcerating skin lesion are presented. Following that, a comparison is made between the finite element model of the skin phantom and the measurements taken on the actual skin model to validate the FE model. The cooling and reheating curves obtained from temperature sensors are displayed and compared with one another. The final section incorporates the decision matrix, providing a comprehensive overview of the various cooling methods, their advantages and disadvantages, and ultimately determining the most suitable cooling method.

3.1. Agar Skin Phantom

Figure 3 illustrates the application of six different cooling methods on the flat agar skin phantoms. The thermograms selected at 5 s into the reheating are displayed. Below each thermogram, the corresponding histograms are shown. The histograms of the vortex cooler and cryo cooler (convective cooling methods) appear relatively narrow and tall, indicating uniform cooling distribution on the skin phantom. Conversely, the cool pack and aluminum medal cooling employ conductive cooling, resulting in wider and less tall histograms compared to the convective cooling methods, suggesting less uniform cooling.

Notably, this figure reveals a significant factor: the ice and alcohol cooling methods interfere with infrared radiation capture. When using ice for cooling, the melting ice leaves a layer of cold water on the skin phantom, which affects the thermal camera's view. The water absorbs and scatters infrared radiation, causing attenuated and out-of-focus thermograms. Similarly, the evaporative cooling effect of alcohol has a profound influence on thermal imaging. The alcohol vapors obstruct the view of the agar skin phantom, rendering it invisible to the thermal camera. Moreover, the application of substances such as ice, water, and alcohol to the skin is undesirable due to their potential impact on skin integrity and functionality.

Because of the influence of ice, water and alcohol on the skin and infrared radiation, these cooling methods are no longer considered for application on the ulcerating skin lesion. The four remaining cooling methods, cool pack, vortex cooler, cryo cooler and an aluminum medal, are again applied on the skin phantom. Figure 4 shows the reheating state 5 s after the cooling is removed. It is clearly visible that the convective cooling

methods (vortex cooler and cryo cooler) create a more uniform cooling in regard to the ulceration. The conductive methods, cool pack and aluminum medal, clearly cool the ulceration but not the area directly around the ulceration. The cool pack and aluminum medal are not able to make contact with the transition between the bulge and the flat skin surrounding it. This is also clearly visible in the corresponding histograms of the reheating thermogram. The thermograms of the convective methods are narrower than the ones of the conductive methods.

Due to the adverse effects of ice, water, and alcohol on the skin and infrared radiation, these cooling methods are no longer considered suitable for application on the skin. Therefore, the four remaining cooling methods, namely cool pack, vortex cooler, cryo cooler, and aluminum medal, were reevaluated and applied to the ulcerating skin phantom. Figure 4 illustrates the reheating state, which was captured 5 s after the cooling was removed. It is evident that the convective cooling methods (vortex cooler and cryo cooler) achieve a more uniform cooling effect specifically around the ulceration. Conversely, the conductive methods, cool pack and aluminum medal, effectively cool the ulceration but do not extend their cooling reach to the surrounding skin area. Notably, the cool pack and aluminum medal fail to establish contact with the transitional region between the bulge and the adjacent flat skin as depicted in thermogram. Furthermore, the histograms obtained from the convective methods exhibit narrower profiles compared to those generated by the conductive methods.

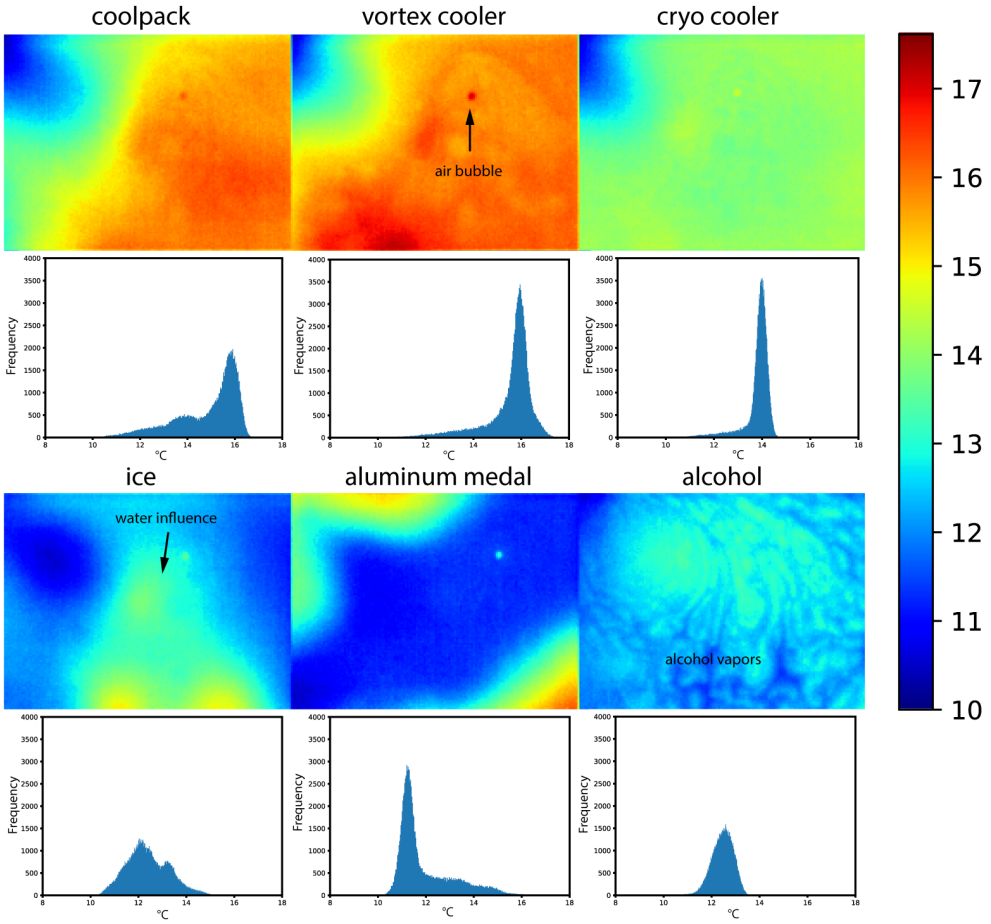

Figure 3. The figure displays the results of six cooling methods along with their corresponding histograms. A round spot visible in the images represents an air bubble, which is an artifact that occurred during the fabrication of the agar phantom. Among the cooling methods, the cool pack, vortex, cryo, and aluminum medal cooling exhibit a more uniform cooling pattern, as evident from the histograms. In contrast, the ice and alcohol cooling methods have a distinct influence on infrared radiation.

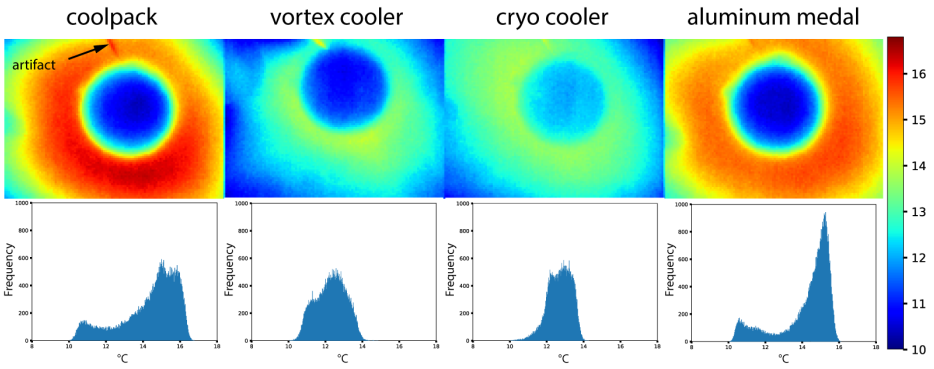

Figure 4. The figure presents the outcomes of the four remaining cooling methods, which were accompanied by their respective histograms. The circular area in the thermogram represents the ulcerating skin lesion. It is evident that the convective cooling methods demonstrate a more uniform cooling effect in contrast to the conductive cooling methods, which encounter challenges in effectively cooling the immediate region surrounding the bulge.

3.2. Temperature Measurements

The flat agar skin phantoms were subjected to 30 s of cooling using six different methods. The temperature measurements were taken at depths of 5 mm and 9 mm using the temperature sensors. The time interval from −5 to 0 s represents the steady-state phase. During this phase, the temperature at a depth of 5mm remains approximately 33 °C, while at a depth of 9 mm, it remains around 37 °C. At 0 s, the cooling sequence is initiated, and after 30 s, the cooling load is removed, marking the beginning of the reheating phase. Figure 5 illustrates the cooling and reheating curves for the various cooling methods. Among them, ice proves to be the fastest at reducing the temperature at a depth of 5 mm. After 30 s of cooling, the temperature at 5 mm is approximately 24 °C and keeps decreasing to a minimum of approx. 21 °C. The cooling effect of the alcohol spray is insufficient for adequately cooling the skin phantom, the cooling is slow and the penetration depth of the cooling is not sufficient. The cryo cooler was employed at three different levels: level 1, level 3, and level 5. As depicted in Figure 5, level 5 demonstrates a more rapid cooling of the skin phantom compared to level 3 and level 1. At a depth of 9 mm, it becomes evident that both ice and the cryo cooler achieve the fastest and deepest cooling. Conversely, the conductive cooling methods, the vortex tube and alcohol spray, do not achieve the same cooling as the cryo cooler and ice.

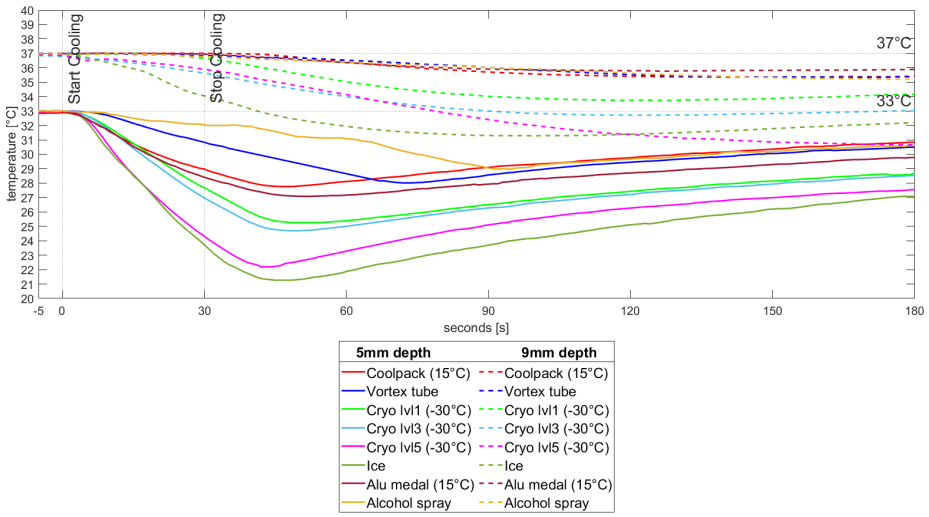

Figure 5. The figure presents the results of applying six different cooling methods on the flat agar skin phantom for a duration of 30 s at 5 mm and 9 mm depth. Among the cooling methods, ice demonstrates the most rapid cooling rate, while alcohol spray shows the slowest cooling performance and fails to achieve sufficient cooling.

3.3. Decision Matrix

Table 2 provides an overview of the scores and rankings for each cooling option based on all criteria. The Zimmer Cryo 6 obtains the highest total weighted points, totaling 160, making it the top-ranked choice. Following closely behind is the vortex tube with 132 weighted points. Conversely, the alcohol spray receives the lowest weighted total among the cooling methods. Notably, the convective cooling methods outperform others, garnering the highest points. The third and fourth positions are occupied by the two conductive cooling methods, excluding ice, which presents the challenge of leaving water that obstructs the camera's view after cooling.

The Zimmer Cryo 6 cooler demonstrates superior performance compared to other cooling methods. It offers several notable advantages, including the ability to uniformly apply cooling to the skin and consistent conditioning of cold air regardless of the device's location or usage. Additionally, the Cryo 6 exhibits high cooling efficiency at −30 °C. Importantly, the cooling process does not obstruct the field of view of the thermal camera, allowing for accurate recording of the skin lesion's cooling sequence. Another noteworthy advantage is that the Cryo 6 does not require additional equipment or consumables, making it user-friendly and minimizing the workload per patient during clinical practice.

4. Conclusions

In conclusion, skin cancer is a significant global health issue, with increasing incidence rates and a substantial impact on both individuals and society. Traditional methods of diagnosis, such as visual examination and biopsy, have limitations in terms of invasiveness and detection accuracy. This has led to the exploration of alternative diagnostic tools such as infrared thermography.

To facilitate research and experimentation in skin cancer diagnosis, tissue-mimicking phantoms have been utilized. These phantoms provide a controlled and reproducible environment for studying skin interactions, overcoming ethical challenges associated with human subjects. While they have limitations in replicating the complex structure and composition of human skin, physical skin models offer stability, ease of fabrication, and control over physical properties. In this research, Agarose phantoms are used. These can be easily fabricated and tailored to mimic specific skin conditions. However, they have limitations in terms of long-term stability and shelf life.

This study aimed to test and compare different cooling techniques for human skin in the context of skin cancer diagnosis using dynamic infrared thermography. Six cooling methods were investigated and categorized into three types: convection cooling, conduction cooling, and evaporative cooling. The experimental setup involved an infrared camera (Optris Xi400) with microscope optics positioned 100 mm above a skin-mimicking agar phantom. The phantom was created using a 4% agar solution and had molds resembling flat skin and an ulcerating skin lesion. The measurement protocol included a cooling period of 60 s followed by a reheating process captured by the thermal camera. Data processing involved preprocessing, segmentation, and the analysis of thermal images using a Python algorithm. Based on the experiments conducted on the skin phantom, it has been observed that convective cooling methods offer a more consistent and uniform cooling effect. On the other hand, conductive methods prove effective in cooling flat objects; however, achieving uniform cooling becomes more challenging when dealing with bulging skin or ulceration skin lesions. Ice or alcohol for cooling purposes is unsuitable when used in conjunction with infrared thermography. This is primarily because the cooling effects of ice or alcohol can introduce artifacts that affect both the infrared radiation and the thermal camera's view, thereby compromising the accuracy and reliability of the results obtained. A decision matrix was used to evaluate and compare the cooling techniques based on criteria such as uniform cooling, repeatability, obstructing the view, cooling efficiency, workload per patient, patient comfort, use in a clinical setting, noise exposure, consumables and additional equipment, and price. The technique with the highest weighted score was considered the best suitable

cooling method for skin cancer diagnosis. After assessing various factors, the Zimmer Cryo 6 cooler emerged as the most suitable cooling method.

The Cryo 6 cooler demonstrated several advantages, including its ability to provide uniform cooling to the skin, consistent conditioning of cold air, and high cooling efficiency at −30 °C. Importantly, it did not obstruct the field of view of the thermal camera, allowing for accurate recording of the skin lesion's cooling sequence. Additionally, the Cryo 6 cooler was user-friendly, as it did not require additional equipment or consumables, reducing the workload during clinical practice. The disadvantage of the Cryo 6 cooler is the price of the device.

The application of active thermography in the identification of various types of cancers holds significant clinical importance. Ongoing research endeavors are directed toward utilizing infrared thermography for the detection of deep-seated cancers, such as breast cancer [59,60]. Additionally, in breast cancer detection studies, skin phantoms find valuable utility [61]. Active thermography exhibits considerable promise in the exploration and characterization of cancer. Currently, there is a substantial focus on researching surface cancers like skin cancer. In contrast, the detection of deep tissue cancers presents greater challenges.

Author Contributions: Conceptualization, J.V. and G.S.; Data curation, J.V.; Funding acquisition, L.B. and G.S.; Investigation, J.V.; Methodology, J.V.; Software, J.V.; Supervision, F.E.F.T. and L.B.; Writing—original draft, J.V.; Writing—review and editing, F.E.F.T., I.H., L.B. and G.S. All authors have read and agreed to the published version of the manuscript.

Funding: This research was funded by the Fonds Wetenschappelijk Onderzoek (FWO) via support for the FWO research project, "Optimized skin tissue identification by combined thermal and hyperspectral imaging methodology" (project number 41882 (FWO G0A9720N)).

Institutional Review Board Statement: The study was conducted in accordance with the Declaration of Helsinki and approved by the local Ethics Committee of the University Hospital Antwerp (B300201941125, date of approval: 16 May 2022).

Informed Consent Statement: Not applicable.

Data Availability Statement: The data presented in this study are available on request from the corresponding author. The data are not yet publicly available. The data are available on request due to project data management limitations.

Conflicts of Interest: The authors declare no conflict of interest.

Abbreviations

The following abbreviations are used in this manuscript:

TBSE	Total body skin examination
DIRT	Dynamic infrared thermography
CT	Computed Tomography
PET	Positron emission tomography
IRT	Infrared Thermography
NETD	Noise Equivalent Temperature Difference
NUC	Non-uniformity correction
IFOV	Instantaneous field of view
MFOV	Measurement field of view
RTD	Resistance Temperature Detector

References

1. World Health Organization. *World Cancer Report: Cancer Research for Cancer Development*; IARC: Lyon, France, 2020.
2. Sung, H.; Ferlay, J.; Siegel, R.L.; Laversanne, M.; Soerjomataram, I.; Jemal, A.; Bray, F. Global Cancer Statistics 2020: GLOBOCAN Estimates of Incidence and Mortality Worldwide for 36 Cancers in 185 Countries. *CA A Cancer J. Clin.* **2021**, *71*, 209–249. [CrossRef] [PubMed]

3. Eisemann, N.; Waldmann, A.; Geller, A.C.; Weinstock, M.A.; Volkmer, B.; Greinert, R.; Breitbart, E.W.; Katalinic, A. Non-Melanoma Skin Cancer Incidence and Impact of Skin Cancer Screening on Incidence. *J. Investig. Dermatol.* **2014**, *134*, 43–50. [CrossRef] [PubMed]
4. Verstockt, J.; Verspeek, S.; Thiessen, F.; Tjalma, W.A.; Brochez, L.; Steenackers, G. Skin Cancer Detection Using Infrared Thermography: Measurement Setup, Procedure and Equipment. *Sensors* **2022**, *22*, 3327. [CrossRef]
5. Johnson, M.M.; Leachman, S.A.; Aspinwall, L.G.; Cranmer, L.D.; Curiel-Lewandrowski, C.; Sondak, V.K.; Stemwedel, C.E.; Swetter, S.M.; Vetto, J.; Bowles, T.; et al. Skin cancer screening: Recommendations for data-driven screening guidelines and a review of the US Preventive Services Task Force controversy. *Melanoma Manag.* **2017**, *4*, 13–37. [CrossRef] [PubMed]
6. Nachbar, F.; Stolz, W.; Merkle, T.; Cognetta, A.B.; Vogt, T.; Landthaler, M.; Bilek, P.; Braun-Falco, O.; Plewig, G. The ABCD rule of dermatoscopy: High prospective value in the diagnosis of doubtful melanocytic skin lesions. *J. Am. Acad. Dermatol.* **1994**, *30*, 551–559. [CrossRef] [PubMed]
7. Brunssen, A.; Waldmann, A.; Eisemann, N.; Katalinic, A. Impact of skin cancer screening and secondary prevention campaigns on skin cancer incidence and mortality: A systematic review. *J. Am. Acad. Dermatol.* **2017**, *76*, 129–139.e10. [CrossRef] [PubMed]
8. Braun, R.P.; Oliviero, M.; Kolm, I.; French, L.E.; Marghoob, A.A.; Rabinovitz, H. Dermoscopy: What's new? *Clin. Dermatol.* **2009**, *27*, 26–34. [CrossRef]
9. Rey-Barroso, L.; Peña-Gutiérrez, S.; Yáñez, C.; Burgos-Fernández, F.J.; Vilaseca, M.; Royo, S. Optical Technologies for the Improvement of Skin Cancer Diagnosis: A Review. *Sensors* **2021**, *21*, 252. [CrossRef]
10. Kirimtat, A.; Krejcar, O.; Selamat, A. A Mini-review of Biomedical Infrared Thermography (B-IRT). In *Bioinformatics and Biomedical Engineering*; Lecture Notes in Computer Science; Rojas, I., Valenzuela, O., Rojas, F., Ortuño, F., Eds.; Springer International Publishing: Cham, Switzerland, 2019; Volume 11466, pp. 99–110. [CrossRef]
11. Qi, H.; Diakides, N. *Infrared Imaging in Medicine*; Technical Report; University of Tennessee: Knoxville, TN, USA, 2007.
12. Flores-Sahagun, J.H.; Vargas, J.V.C.; Mulinari-Brenner, F.A. Analysis and diagnosis of basal cell carcinoma (BCC) via infrared imaging. *Infrared Phys. Technol.* **2011**, *54*, 367–378. [CrossRef]
13. Buzug, T.M.; Schumann, S.; Pfaffmann, L.; Reinhold, U.; Ruhlmann, J. Functional infrared imaging for skin-cancer screening. In Proceedings of the Annual International Conference of the IEEE Engineering in Medicine and Biology—Proceedings, New York, NY, USA, 30 August–3 September 2006; pp. 2766–2769. [CrossRef]
14. Jiang, L.J.; Ng, E.Y.K.; Yeo, A.C.B.; Wu, S.; Pan, F.; Yau, W.Y.; Chen, J.H.; Yang, Y. A perspective on medical infrared imaging. *J. Med. Eng. Technol.* **2005**, *29*, 257–267. [CrossRef]
15. Moustafa, A.M.N.; Muhammed, H.H.; Hassan, M. Skin Cancer Detection Using Temperature Variation Analysis. *Engineering* **2013**, *5*, 18–21. [CrossRef]
16. Chen, H.; Wang, K.; Du, Z.; Liu, W.; Liu, Z. Predicting the thermophysical properties of skin tumor based on the surface temperature and deep learning. *Int. J. Heat Mass Transf.* **2021**, *180*, 121804. [CrossRef]
17. Dąbrowska, A.K.; Rotaru, G.M.; Derler, S.; Spano, F.; Camenzind, M.; Annaheim, S.; Stämpfli, R.; Schmid, M.; Rossi, R.M. Materials used to simulate physical properties of human skin. *Skin Res. Technol.* **2016**, *22*, 3–14. [CrossRef] [PubMed]
18. Pogue, B.W.; Patterson, M.S. Review of tissue simulating phantoms for optical spectroscopy, imaging and dosimetry. *J. Biomed. Opt.* **2006**, *11*, 041102. [CrossRef]
19. Dabbagh, A.; Abdullah, B.J.J.; Ramasindarum, C.; Abu Kasim, N.H. Tissue-Mimicking Gel Phantoms for Thermal Therapy Studies. *Ultrason. Imaging* **2014**, *36*, 291–316. [CrossRef]
20. Shevchenko, R.V.; James, S.L.; James, S.E. A review of tissue-engineered skin bioconstructs available for skin reconstruction. *J. R. Soc. Interface* **2009**, *7*, 229–258. [CrossRef]
21. Ohmae, E.; Yoshizawa, N.; Yoshimoto, K.; Hayashi, M.; Wada, H.; Mimura, T.; Suzuki, H.; Homma, S.; Suzuki, N.; Ogura, H.; et al. Stable tissue-simulating phantoms with various water and lipid contents for diffuse optical spectroscopy. *Biomed. Opt. Express* **2018**, *9*, 5792–5808. [CrossRef]
22. Lamouche, G.; Kennedy, B.F.; Kennedy, K.M.; Bisaillon, C.E.; Curatolo, A.; Campbell, G.; Pazos, V.; Sampson, D.D. Review of tissue simulating phantoms with controllable optical, mechanical and structural properties for use in optical coherence tomography. *Biomed. Opt. Express* **2012**, *3*, 1381–1398. [CrossRef]
23. Nordstrom, R.J. Phantoms as standards in optical measurements. In Proceedings of the Optical Diagnostics and Sensing XI: Toward Point-of-Care Diagnostics; and Design and Performance Validation of Phantoms Used in Conjunction with Optical Measurement of Tissue III, SPIE, San Francisco, CA, USA, 26 January 2011; Volume 7906, pp. 75–79. [CrossRef]
24. Çetingül, M.P.; Herman, C. A heat transfer model of skin tissue for the detection of lesions: Sensitivity analysis. *Phys. Med. Biol.* **2010**, *55*, 5933–5951. [CrossRef]
25. Koehler, M.J.; Vogel, T.; Elsner, P.; König, K.; Bückle, R.; Kaatz, M. In vivo measurement of the human epidermal thickness in different localizations by multiphoton laser tomography. *Skin Res. Technol.* **2010**, *16*, 259–264. [CrossRef]
26. Birgersson, U.; Birgersson, E.; Nicander, I.; Ollmar, S. A methodology for extracting the electrical properties of human skin. *Physiol. Meas.* **2013**, *34*, 723–736. [CrossRef] [PubMed]
27. Krackowizer, P.; Brenner, E. Thickness of the human skin. *Phlebologie* **2008**, *37*, 83–92. [CrossRef]
28. Sontheimer, R.D. Skin Is Not the Largest Organ. *J. Investig. Dermatol.* **2014**, *134*, 581–582. [CrossRef] [PubMed]
29. Venus, M.; Waterman, J.; McNab, I. Basic physiology of the skin. *Surgery* **2010**, *28*, 469–472. [CrossRef]

30. Yoo, H.; Hu, Y.; Kim, E. Effects of Heat and Moisture Transport in Fabrics and Garments Determined with a Vertical Plate Sweating Skin Model. *Text. Res. J.* **2000**, *70*, 542–549. [CrossRef]
31. Wang, F.; del Ferraro, S.; Lin, L.Y.; Sotto Mayor, T.; Molinaro, V.; Ribeiro, M.; Gao, C.; Kuklane, K.; Holmér, I. Localised boundary air layer and clothing evaporative resistances for individual body segments. *Ergonomics* **2012**, *55*, 799–812. [CrossRef] [PubMed]
32. Kim, J. Dynamic Moisture Vapor Transfer Through Textiles: Part III: Effect of Film Characteristics on Microclimate Moisture and Temperature Changes. *Text. Res. J.* **1999**, *69*, 193–202. [CrossRef]
33. Huang, J.; Holt, R.G.; Cleveland, R.O.; Roy, R.A. Experimental validation of a tractable numerical model for focused ultrasound heating in flow-through tissue phantoms. *J. Acoust. Soc. Am.* **2004**, *116*, 2451–2458. [CrossRef]
34. Ambastha, S.; Pant, S.; Umesh, S.; Vazhayil, V.; Asokan, S. Feasibility Study on Thermography of Embedded Tumor Using Fiber Bragg Grating Thermal Sensor. *IEEE Sensors J.* **2020**, *20*, 2452–2459. [CrossRef]
35. Çetingül, M.P.; Herman, C. Using Dynamic Infrared Imaging to Detect Melanoma: Experiments on a Tissue-Mimicking Phantom. In *Volume 2: Biomedical and Biotechnology Engineering*; ASMEDC: Vancouver, BC, Canada, 2010; pp. 139–147. [CrossRef]
36. Kumari, C.; Kumar, A.; Sarangi, S.K.; Thirugnanam, A. An experimental and numerical study for cutaneous cryotherapy. *Heat Mass Transf.* **2021**, *57*, 147–163. [CrossRef]
37. Cho, J.; Prasad, B.; Kim, J.K. Near-infrared laser irradiation of a multilayer agar-gel tissue phantom to induce thermal effect of traditional moxibustion. *J. Innov. Opt. Health Sci.* **2018**, *11*, 1850033. [CrossRef]
38. Hou, S. Photo-Thermally Enhanced Temperature Gradient Gel Electrophoresis for DNA Separation. Ph.D. Thesis, Northeastern University, Boston, MA, USA, 2018.
39. Zenzie, H.; Altshuler, G.; Smirnov, M.; Anderson, R. Evaluation of cooling methods for laser dermatology. *Lasers Surg. Med.* **2000**, *26*, 130–144. [CrossRef]
40. Cheng, T.Y.; Herman, C. Analysis of skin cooling for quantitative dynamic infrared imaging of near-surface lesions. *Int. J. Therm. Sci.* **2014**, *86*, 175–188. [CrossRef]
41. Strąkowska, M.; Strzelecki, M.; Kaszuba, A. Novel methodology of medical screening using IR thermography. In Proceedings of the 2014 Signal Processing: Algorithms, Architectures, Arrangements, and Applications (SPA), Poznan, Poland, 22–24 September 2014; pp. 172–175.
42. Buzug, T.; Schumann, S.; Pfaffmann, L.; Reinhold, U.; Ruhlmann, J. Skin-Tumour Classification with Functional Infrared Imaging. In Proceedings of the 8th IASTED International Conference on Signal and Image Processing, SIP 2006, Atlanta, GA, USA, 8–11 October 2006.
43. Santa Cruz, G.A.; Bertotti, J.; Marín, J.; González, S.J.; Gossio, S.; Alvarez, D.; Roth, B.M.C.; Menéndez, P.; Pereira, M.D.; Albero, M.; et al. Dynamic infrared imaging of cutaneous melanoma and normal skin in patients treated with BNCT. *Appl. Radiat. Isot.* **2009**, *67*, S54–S58. [CrossRef] [PubMed]
44. Çetingül, M.P.; Alani, R.M.; Herman, C. Quantitative Evaluation of Skin Lesions Using Transient Thermal Imaging. In Proceedings of the 2010 14th International Heat Transfer Conference, Washington, DC, USA, 8–13 August 2010; ASMEDC: Washington, DC, USA, 2010; Volume 1, pp. 31–39. [CrossRef]
45. Xue, Y.; Arjomandi, M.; Kelso, R. A critical review of temperature separation in a vortex tube. *Exp. Therm. Fluid Sci.* **2010**, *34*, 1367–1374. [CrossRef]
46. Godoy, S.E.; Hayat, M.M.; Ramirez, D.A.; Myers, S.A.; Padilla, R.S.; Krishna, S. Detection theory for accurate and non-invasive skin cancer diagnosis using dynamic thermal imaging. *Biomed. Opt. Express* **2017**, *8*, 2301–2323. [CrossRef]
47. Godoy, S.E.; Ramirez, D.A.; Myers, S.A.; Von Winckel, G.; Krishna, S.; Berwick, M.; Padilla, R.S.; Sen, P.; Krishna, S. Dynamic infrared imaging for skin cancer screening. *Infrared Phys. Technol.* **2015**, *70*, 147–152. [CrossRef]
48. Magalhaes, C.; Vardasca, R.; Rebelo, M.; Valenca-Filipe, R.; Ribeiro, M.; Mendes, J. Distinguishing melanocytic nevi from melanomas using static and dynamic infrared thermal imaging. *J. Eur. Acad. Dermatol. Venereol.* **2019**, *33*, 1700–1705. [CrossRef]
49. Gomboc, T.; Iljaž, J.; Wrobel, L.C.; Hriberšek, M.; Marn, J. Design of constant temperature cooling device for melanoma screening by dynamic thermography. *Eng. Anal. Bound. Elem.* **2021**, *125*, 66–79. [CrossRef]
50. Bonmarin, M.; Gal, F.A.L. A lock-in thermal imaging setup for dermatological applications. *Skin Res. Technol.* **2015**, *21*, 284–290. [CrossRef]
51. Bonmarin, M.; Le Gal, F.A. Chapter 31—Thermal Imaging in Dermatology. In *Imaging in Dermatology*; Hamblin, M.R., Avci, P., Gupta, G.K., Eds.; Academic Press: Boston, MA, USA, 2016; pp. 437–454. [CrossRef]
52. Burkes, S.A.; Patel, M.; Adams, D.M.; Hammill, A.M.; Eaton, K.P.; Randall Wickett, R.; Visscher, M.O. Infantile hemangioma status by dynamic infrared thermography: A preliminary study. *Int. J. Dermatol.* **2016**, *55*, e522–e532. [CrossRef] [PubMed]
53. Cryo 6 Brochure—Information about the Zimmer Skin Cooling Chiller. Available online: https://zimmerusa.com/products/cryo-therapy/cryo-6/cryo-6-brochure/ (accessed on 28 May 2023).
54. Armisén, R.; Gaiatas, F. Agar. In *Handbook of Hydrocolloids*, 2nd ed.; Phillips, G.O., Williams, P.A., Eds.; Woodhead Publishing Series in Food Science, Technology and Nutrition; Woodhead Publishing: Sawston, UK, 2009; pp. 82–107. [CrossRef]
55. in 't Hout, F.E.M.; Haydu, L.E.; Murali, R.; Bonenkamp, J.J.; Thompson, J.F.; Scolyer, R.A. Prognostic Importance of the Extent of Ulceration in Patients With Clinically Localized Cutaneous Melanoma. *Ann. Surg.* **2012**, *255*, 1165. [CrossRef] [PubMed]
56. Grande Sarpa, H.; Reinke, K.; Shaikh, L.; Leong, S.P.L.; Miller, J.R.I.; Sagebiel, R.W.; Kashani-Sabet, M. Prognostic Significance of Extent of Ulceration in Primary Cutaneous Melanoma. *Am. J. Surg. Pathol.* **2006**, *30*, 1396. [CrossRef] [PubMed]

57. Ullman, D.G. *The Mechanical Design Process*, 4th ed.; McGraw-Hill Series in Mechanical Engineering; McGraw-Hill Higher Education: Boston, MA, USA, 2010.
58. Tague, N.R. *The Quality Toolbox*, 2nd ed.; ASQ Quality Press: Milwaukee, WI, USA, 2005.
59. Figueiredo, A.A.A.; do Nascimento, J.G.; Malheiros, F.C.; da Silva Ignacio, L.H.; Fernandes, H.C.; Guimaraes, G. Breast tumor localization using skin surface temperatures from a 2D anatomic model without knowledge of the thermophysical properties. *Comput. Methods Programs Biomed.* **2019**, *172*, 65–77. [CrossRef] [PubMed]
60. Gershenson, M.; Gershenson, J. Dynamic Vascular Imaging Using Active Breast Thermography. *Sensors* **2023**, *23*, 3012. [CrossRef]
61. Sadeghi, M.; Boese, A.; Maldonado, I.; Friebe, M.; Sauerhering, J.; Schlosser, S.; Wehberg, H.; Wehberg, K. Feasibility test of Dynamic Cooling for detection of small tumors in IR thermographic breast imaging. *Curr. Dir. Biomed. Eng.* **2019**, *5*, 397–399. [CrossRef]